Absorption-induced trapping in an anisotropic magneto-optical trap

Joel A. Greenberg,[1] **M. Oriá,**[1,2] **Andrew M.C. Dawes,**[1] **and**
Daniel J. Gauthier[1]

[1]*Physics Department, Science Drive, Duke University, Durham, NC, 27708*
[2]*Lab. de Física Atômica e Lasers-Departamento de Física - CCEN Universidade Federal da
Paraíba - Cx Postal 5008 - 58051-970 - João Pessoa, PB Brazil*
jag27@phy.duke.edu

Abstract: We report on a simple anisotropic magneto-optical trap for neutral atoms that produces a large sample of cold atoms confined in a cylindrically-shaped volume with a high aspect ratio (100:1). Due to the large number of trapped atoms, the laser beams that propagate along the optically thick axis of the trap to cool the atoms are substantially attenuated. We demonstrate that the resulting intensity imbalance produces a net force that spatially localizes the atoms. This limits both the trap length and the total number of trapped atoms. Rotating the cooling beams by a small angle relative to the trap axis avoids the problem of attenuation, and atoms can be trapped throughout the entire available trapping volume. Numerical and experimental results are reported that demonstrate the effects of absorption in an anisotropic trap, and a steady-state, line-center optical path length of 55 is measured for a probe beam propagating along the length of the trap.

OCIS codes: (020.3320) Laser cooling; (020.7010) Laser trapping; (190.0190) Nonlinear optics.

References and links

1. A. Lambrecht, T. Coudreau, A.M. Steinberg, E. Giacobino, "Squeezing with Cold Atoms," Europhys. Lett. **36**, 93 (1996).
2. G. Labeyrie, G.L. Gattobigio, T. Chaneliére, G.L. Lippi, T. Ackemann, R. Kaiser, "Nonlinear Lensing Mechanisms in a Cloud of Cold Atoms," Euro. Phys. Jn. D. **41**, 337 (2007).
3. Y. Wang, M. Saffman, "Experimental Study of Nonlinear Focusing in a Magneto-optical Trap Using a Z-scan Technique," Phys. Rev. A **70**, 013801 (2004).
4. M. Vengalatorre, M. Prentiss, "Radial Confinement of Light in an Ultracold Anisotropic Medium," Phys. Rev. Lett. **95**, 243601 (2005).
5. G.L. Gattobigio, F. Michaud, J. Javaloyes, J.W.R. Tabosa, R. Kaiser, "Bunching-induced Asymmetry in Degenerate Four-wave Mixing with Cold Atoms," Phys. Rev. A **74**, 043407 (2006).
6. K.R. Hansen, K. Mølmer, "Trapping of Light Pulses in Ensembles of Stationary Λ Atoms," Phys. Rev. A **75**, 053802 (2007).
7. H.W. Chan, A.T. Black, V. Vuletić, "Observation of Collective-Emission-Induced Cooling of Atoms in an Optical Cavity," Phys. Rev. Lett. **90**, 063003 (2003).
8. A.T. Black, H.W. Chan, V. Vuletić, "Observation of Collective Friction Forces due to Spatial Self-Organization of Atoms: From Rayleigh to Bragg Scattering," Phys. Rev. Lett. **91**, 203001 (2003).
9. R. Bonificio, L. De Salvo, "Collective Atomic Recoil Laser (CARL) Optical Gain Without Inversion by Collective Atomic Recoil and Self-bunching of Two-level Atoms," Nucl. Instrum. Methods Phys. Res. Sec. A **341**, 360 (1994).
10. G. Grynberg, C. Robbiliard, "Cold Atoms in Dissipative Optical Lattices," Phys. Rep. **3**, 355 (2001).
11. W. Ketterle, K. Davis, M. Joffe, A. Martin, D. Pritchard, "High Densities of Cold Atoms in a Dark Spontaneous-Force Optical Trap," Phys. Rev. Lett. **70**, 2253 (1993).

12. K.E. Gibble, S. Kasapi, S. Chu, "Improved Magneto-optic trapping in a Vapor Cell," Opt. Lett. **17**, 526 (1992).
13. Y. Castin, J.I. Cirac, M. Lewenstein, "Reabsorption of Light by Trapped Atoms," Phys. Rev. Lett. **80**, 5305 (1998).
14. M. Vengalatorre, W. Rooijakkers, M. Prentiss, "Ferromagnetic Atom Guide with In Situ Loading," Phys. Rev. A **66**, 053403 (2002).
15. M. Vengalatorre, W. Rooijakkers, R. Conroy, M. Prentiss, "Suppression of Photon Rescattering due to Spatial Anisotropy in a Cold Atomic Gas," Phys. Rev. A **67**, 063412 (2003).
16. M. Vengalatorre, M. Prentiss, "Recoil-induced Resonances in the High-gain Regime," Phy. Rev. A, **72**, 1(R) (2005).
17. T. Ackemann, W. Lange, "Optical Pattern Formation in Alkali Metal Vapors: Mechanisms, Phenomena and Use." Appl. Phys. B **72**, 21 (2001).
18. A.M.C. Dawes, L. Illing, S. M. Clark, D. J. Gauthier, "All Optical Switching in Rubidium Vapor," Science **308**, 672 (2005).
19. S. Wu, E. Su, M. Prentiss, "Time Domain de Broglie Wave Interferometry Along a Magnetic Guide," Eur. Phys. J. D. **35**, 111 (2005).
20. K. L. Corwin, Z. Lu, C. F. Hand, R. J. Epstein, and C. E. Wieman, "Frequency-Stabilized Diode Laser with the Zeeman Shift in an Atomic Vapor," Appl. Opt. **37**, 3295 (1998).
21. E.A. Donley, T.P. Heavner, F. Levi, M.O. Tataw, S.R. Jefferts, "Double-pass Acousto-optic Modulator System," Rev. Sci. Inst. **76**, 063112 (2005).
22. J. Dalibard, "Laser Cooling of an Optically Thick Gas: The Simplest Radiation Pressure Trap?," Opt. Commun. **68**, 203 (1988).
23. M. Vengalatorre, *private communication* (2007).
24. H. J. Metcalf, P. van der Straten, "Laser Cooling and Trapping," (Springer-Verlag, New York, NY, 1999), Ch. 11.4.2.
25. J. Guo, P.R. Berman, B. Dubetsky, "Recoil-induced Resonances in Nonlinear Spectroscopy," Phys. Rev. A **46**, 1426 (1993).
26. M. Brzozowska, T. Brzozowski, J. Zachorowski, W. Gawlik, "Nondestructive Study of Nonequilibrium States of Cold Trapped Atoms," Phys. Rev. A **72**, 061401 (2005).

1. Introduction

It is well known that nonlinear optical effects can be enhanced by tuning the frequency of light passing through a medium close to a material resonance. Despite this resonant enhancement, the negative effects of strong linear absorption near resonance require a compromise between working too near or far from a resonance. In a medium consisting of a warm vapor, inhomogeneous Doppler broadening produces linewidths that are typically a factor of 100 larger than the homogeneous linewidth; thus, substantial absorption occurs over a large bandwidth and the atom-photon coupling is reduced. In a cold atomic sample, on the other hand, the atomic linewidth is on-the-order-of the natural linewidth because of the quasi-stationary character of the atoms. This allows researchers to either achieve fully saturated nonlinearities with a weaker probe beam or realize new phenomena. Furthermore, tuning close to resonance can mean that light only strongly interacts with a small number of atomic transitions, thus allowing for simpler, more accurate modeling of the interaction.

In addition to allowing 'cleaner' experimental investigations of previously studied nonlinearities (*i.e.* squeezed light [1], nonlinear beam shaping [2, 3], slow light [4], and nonlinear wave mixing [5]), cold atoms enable new types of nonlinearities. They allow longer-lasting coherences to be established in a sample, which enables the realization of light trapping schemes for quantum information processing [6]. Also, because of the more pronounced effects of momentum transfer on cold atoms, collective effects resulting in the interplay between the atomic density distribution and optical nonlinearities can result in enhanced emission [7, 8], collective atomic recoil lasing (CARL) [9], and Bragg scattering [10]. Unfortunately, the potential benefits of investigating nonlinear optical processes in cold atom systems have typically been outweighed by the fact that a standard (spherical) magneto-optical trap (MOT) traditionally has a peak density of $10^9 - 10^{11}$ atoms/cm^3 and an interaction length of several mm. On the other hand, warm vapors typically enable one to achieve stronger nonlinearities, as they can be
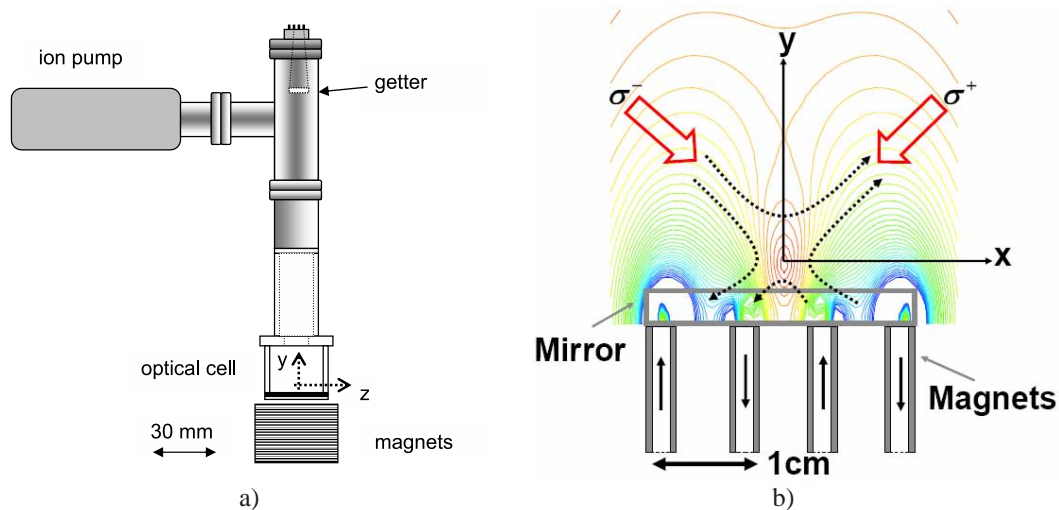
Fig. 1. a) The atom trap setup. b) Magnetic field contours (0.6 G/line) resulting from the magnetic cores (only a portion of the cores is shown). The orientation and polarization of the trapping beams (red arrows) are also shown, along with the orientation of the quadrupolar field lines.

prepared with densities of $> 10^{14}$ atoms/cm^3 and interaction lengths on the order of several cm.

While several techniques have been proposed to increase the density in a spherical MOT [11, 12], density limitations of 10^{12} atoms/cm^3 are ultimately imposed by radiation pressure effects due to the reabsorption of scattered light. To reduce the effects of reabsorption within the trap volume and, thereby, increase the maximum achievable optical depth [OD; $I_i/I_f = exp(-OD)$ where I_i (I_f) is the initial (final) intensity], Castin *et al.* [13] proposed using strongly deformed traps (either cigar-shaped or pancake-shaped). Vengalatorre *et al.* verified that photon rescattering is essentially not important in a 1D sample [15] and were able to achieve densities of $\sim 10^{11}$ atoms/cm^3 over several centimeters. Thus, with an anisotropic trap, one can create an atomic sample with an OD that is comparable to that of a warm vapor, while making use of all of the advantages of cold atoms. With such a system, new work can be done to investigate recoil-induced resonances in the high gain regime [16], pattern forming optical instabilities [17], non-EIT based all-optical switching [16, 18], and atom interferometry [19], which require ODs beyond those achievable in a traditional spherical MOT.

One new issue faced by anisotropic traps with large ODs is the occurrence of absorption-induced forces along the optically thick axis of the trap. As the OD of the trap increases, an intensity imbalance between beams that counterpropagate along the optically thick axis of the trap develops due to the attenuation of the beams. This produces a spatial localization of the atoms that limits the maximum optical depth obtainable. In this paper, we give experimental results that demonstrate the effects of absorption on the formation and steady-state behavior of the trap, as well as provide a numerical model to confirm our interpretation of the results. Furthermore, we demonstrate a technique for avoiding absorption-induced forces that allows us to produce a sample of cold atoms with a large OD.

The outline of the paper is as follows: Section 2 describes the experimental setup, Sec. 3 details the numerical model developed, and results and discussions are presented in Sec. 4.

2. Experimental setup

In our experiment, a simple setup (which is similar to that of Vengalatorre *et al.* [14]) is used to trap ^{87}Rb from a room temperature background vapor. We construct a cell using glass windows (3 cm square $\times$ 3 mm thick, Esco Q912125) as walls and a front-surface gold mirror (Esco ZQ715125C) as the base, which are joined using ultra-high-vacuum epoxy (TRA-BOND BA-2116). The top of the cell is connected to a glass cylinder that is, in turn, connected to an ion pump and Rb dispenser casing via a glass-to-metal transition. Figure 1(a) shows a simplified diagram of the vacuum system and cell along with the placement of the magnets (discussed below). We use the ion pump to maintain a background pressure of $< 5 \times 10^{-9}$ Torr and the getter is run at 4 A to release Rb into the cell. After running the getter until the trap forms (5-10 minutes), it does not need to be run for the remainder of the experiment, although we find that running the getter at a lower current (3 A) results in the most dense traps.

To produce the quadrupolar magnetic trapping field (which is effectively independent of the longitudinal z-position) in the transverse $x - y$-plane, we use four high-susceptibility ferromagnetic cores (μ-metal, CO-NETIC AA Sheet CP025-30-14) located external to the vacuum system and directly under the cell. Because the magnets are outside of the vacuum system, it is very simple to reorient or modify them (and, in turn, modify the trap location). Figure 1(b) illustrates the placement of the magnetic cores relative to the mirror as well as the resulting contours of constant magnetic field in the $x - y$-plane. Also, Fig. 1(b) shows that the quadrupolar nature of the field (and, therefore, the field gradient) is oriented along lines that are at 45° to the x- and y-axes. This direction coincides with the trapping beam orientation. The μ-metal cores (5 cm $\times$ 5 cm $\times$ 0.64 mm) are separated from one another by 1 cm; this is 10 times larger than the cores used by Vengalatorre *et al.*, and allows for a larger trapping volume. Each core is wrapped by 200 turns of 20 gauge copper transformer wire to produce the magnetic fields. We use independent current supplies for the inner and outer pairs of coils to vary either the magnitudes of the currents in the coils or their ratio while keeping the current in one pair fixed. The cores are alternately poled and the current ratio between the inner and outer pair is usually $I_{outer}/I_{inner} = 2$ with $I_{outer} = 400$ mA. With this configuration, we can produce a typical gradient of 10 G/cm with a magnetic-field zero along the entire length of the cell at a height of 3 mm above the mirror. The location of the field minimum and the magnetic-field gradient can be adjusted by varying the ratio and magnitude of the currents, respectively.

To produce the trapping and cooling beams, we use a Ti:sapphire laser, which is red detuned from the $5S_{1/2}(F = 2) \leftrightarrow 5P_{3/2}(F = 3)$ cycling transition by two transitional linewidths, Γ (for $\Gamma/2\pi = 6$ MHz at FWHM). Also, to keep population from accumulating in the $F = 1$ state, we use a repump beam from a diode laser, which is tuned to the $5S_{1/2}(F = 1) \leftrightarrow 5P_{3/2}(F = 2)$ transition and propogates along the cooling beam direction. The diode laser is locked to the appropriate atomic line using a DAVLL active feedback system [20]. The beam geometry, shown in Fig. 2(a), consists of two counterpropogating beams (the trapping beams) that are circularly polarized opposite to one another and then reflected off the gold mirror base at 45° in the transverse plane. The trapping beams have a semimajor and semiminor axis of 1.5 cm and 1 cm (defined in the plane perpendicular to the beam's wave vector, with the semimajor axis along the z-axis), and an intensity of 7 mW/cm^2. We use another pair of counterpropogating beams (the cooling beams) to cool the atoms in the z-direction. By using wave plates in various orientations relative to the polarization direction of the cooling beams, we have determined that the polarization of the cooling beams has no effect on the trap. This insensitivity to the the cooling beam polarization verifies that there is no magneto-optical trapping along the longitudinal direction. The cooling beams have a diameter of 1 cm, an intensity of 7 mW/cm^2, and can be rotated about the y-axis (the rotation angle in the $x - z$-plane relative to the z-axis is denoted by θ). Finally, we split off a portion of the main Ti:sapphire beam for use as a probe beam
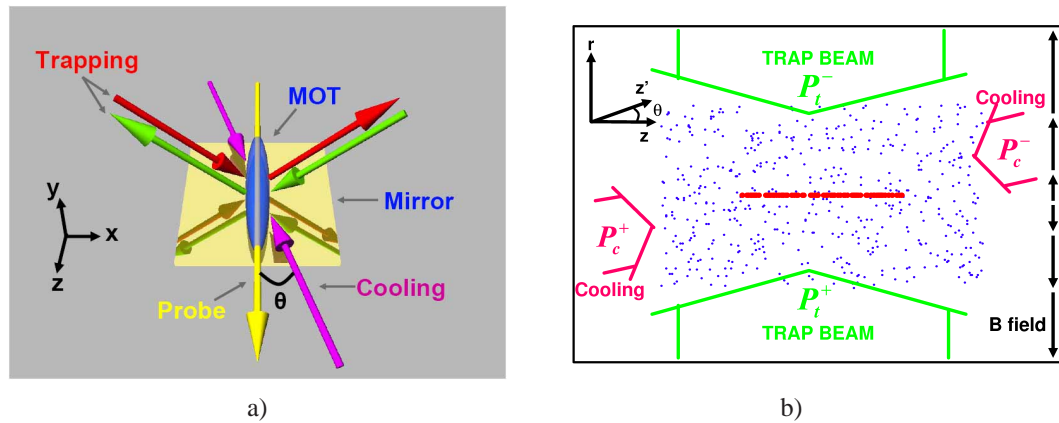
Fig. 2. a) The experimental beam geometry. The trapping beams are in the $x-y$-plane oriented at $45°$ to the y-axis and the cooling beams are in the $x-z$-plane. b) The model beam geometry with effective cooling and trapping beams shown. Also, the relative direction and magnitude of the magnetic field are shown.

($I_{probe} = 100\,\mu\text{W/cm}^2$) that propogates along the z-axis.

To control the amplitude of the trapping and cooling beams and the frequency of the probe beam, we use acousto-optic modulators (AOs; IntraAction, 230 ± 40 MHz). Also, we double-pass the probe beam through an AO [21], which enables us to scan the probe several tens of MHz about the trap beam frequency with negligible angular displacement within the trapping region.

To image the trap, we use two CCD cameras (one viewing the trap horizontally and the other vertically), which give us information on the spatial orientation and dimensions of the trap. Also, we calibrated the horizontal camera by directing a known power onto the CCD, and we use this power to normalize the fluorescence power emitted by the trap (independent of the contrast of the camera). We then extract the number of atoms trapped from the fluorescence power. Additionally, we measure the absorption spectrum of the weak probe beam with a photomultiplier tube (PMT; Hamamatsu H6780-20) to determine the OD of the sample.

3. Absorption-induced trapping mechanism

In general, the mechanisms involved in a MOT are well understood. To describe the observed phonemena, it is usually sufficient to consider the classical forces resulting from an atom with a given velocity and position interacting with red detuned laser beams, in conjunction with the effective detuning due to the Doppler effect and Zeeman level splittings. In the classical picture of atom-photon interactions, the trap location consists of either the locus of points associated with stable orbits or the locations in which force balance occurs.

From this classical picture, it is easy to incorporate the effects of laser beam intensity imbalances in determining where a trap will form. An atom in the presence of counterpropagating beams will preferentially absorb photons from a more intense beam, and will thereby see a net force in the direction of the stonger beam's wave vector. Position-dependent intensity imbalances, due either to beam focusing or absorption effects, have been considered as a mechanism for spatial confinement of cold atoms [22]. In this paper, we ignore the effects of beam focusing (we consider all beams to be perfectly collimated), and concentrate on the effects of absorption on the MOT beams.

Absorption of a beam through a homogeneous, optically thick sample of atoms produces an exponential decrease in beam intensity which follows Beer's law as $I(r)/I(0) = exp(-\int_0^r N[r']\sigma\hat{k} \cdot d\vec{r'})$ where $N[r']$ is the density of atoms at r', σ is the effective absorption cross section, and $\hat{k} \cdot d\vec{r'}$ is a small interval along the beam's propogation direction. If the OD (OD$= \int_0^r N[r']\sigma\hat{k} \cdot d\vec{r'}$) is small, then very little absorption occurs and a beam passes through the sample unattenuated. Under the assumption that the OD is small, the cooling beams in our experiment are predicted to produce only a damping force along the longitudinal direction of the trap. If, instead, one allows for the possibility of ODs that are large enough to produce significant attenuation, then the intensity-dependent absorption force can result in spatial trapping.

We developed a 2D Monte Carlo simulation of the trapping and cooling process to qualitatively model the dynamics of trap formation. Figure 2(b) shows the beam and magnetic-field geometry used for the numerical model as well as the initial (blue) and final (red) positions of the particles. Two sets of counterpropagating Gaussian beams are included in the model, with the trapping beams along the r-direction and the cooling beams along the z'-direction (*i.e.*, at an angle θ relative to the z-axis). The magnetic field is independent of z and has a constant gradient along the r-direction. Thus, our model can effectively capture the full 3 dimensional trapping dynamics because the magnetic field in the experiment can be treated as cylindrically symmetric with an effectively constant gradient along a line in the transverse plane through the field minimum. While optical pumping is ignored, we explicitly incorporate the polarization-selective absorption necessary for spatial trapping due to the Zeeman effect via the probabilities associated with the absorption of a photon from the four laser beams.

In the model, 500 atoms are given random initial positions throughout a fixed volume and assigned random velocities (below a cutoff of 3.5 m/s) that are weighted by a Maxwell-Boltzmann distribution (with $v_{rms} = 350$ m/s). At each time step (which is chosen to be long enough that the probability of absorption is nearly unity), each atom absorbs a photon from one of the laser beams and receives a momentum kick in the corresponding direction. The probability of excitation of an atom due to a monochromatic field is calculated using the rotating-wave and dipole approximations. The probabilities corresponding to the right/up (+) and left/down (-) propagating cooling (c) and trapping (t) beams are given by

$$P_t^{\pm}(r,z) = \frac{1/4(\Omega_t^{\pm})^2}{(\Gamma/2)^2 + 1/2(\Omega_t^{\pm})^2 + (\delta \mp \mathbf{k_t} \cdot \mathbf{v} \mp \mu_B B/\hbar)^2}, \tag{1}$$

$$P_c^{\pm}(r,z) = \frac{1/4(\Omega_c^{\pm})^2}{(\Gamma/2)^2 + 1/2(\Omega_c^{\pm})^2 + (\delta \mp \mathbf{k_c} \cdot \mathbf{v})^2}, \tag{2}$$

where $\delta = \omega - \omega_0$ is the laser detuning, ω_0 is the atomic resonance frequency, $\mathbf{k_{t,c}}$ are the trapping (t) and cooling (c) beam wavevectors, $\mathbf{v}$ is the atom's velocity, and μ_B and $\hbar$ are the Bohr magneton and Planck's constant, respectively. The Rabi frequency for each beam is defined as

$$(\Omega_t^{\pm})^2 = \frac{2I_t^{\pm}|d|^2}{c\varepsilon_0\hbar^2}exp(-z^2/w_t^2), \tag{3}$$

$$(\Omega_c^{\pm})^2 = \frac{2I_c^{\pm}|d|^2}{c\varepsilon_0\hbar^2}exp(-r'^2/w_c^2)exp(\mp n[z']\sigma), \tag{4}$$

where $I_{t,c}^{\pm}$ are the initial intensities of the counterpropagating trapping and cooling beams (before they enter the trapping region), d is the dipole matrix element for the transition, and $w_{t,c}$ are the beam waists of the trapping and cooling beams, respectively. We define the intensity as $I = (1/2)\varepsilon_0 c|E_0|^2$ where $E = E_0\cos(\omega t)$ is the electric field, c is the speed of light in vacuum, and ε_0 is the permittivity of free space. Finally, $B = A \cdot r$ represents the magnetic field along the
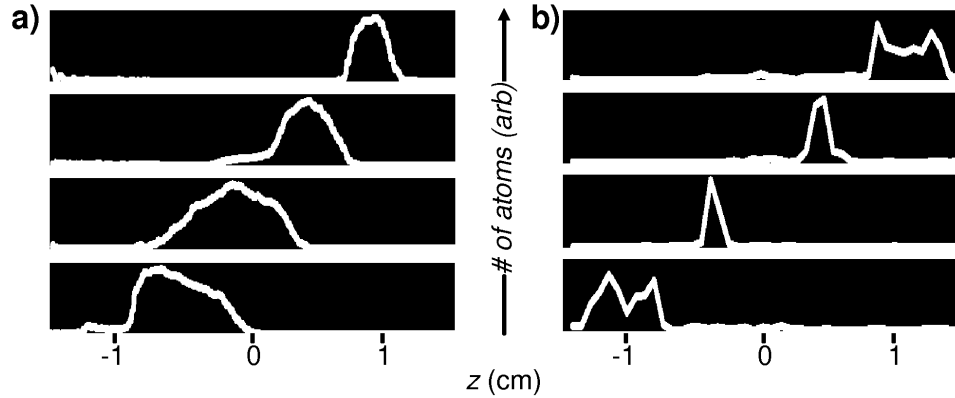
Fig. 3. The effect of the cooling beam intensity imbalance on trap formation. a1)-a4) Experimental longitudinal atomic density profiles that result when $\theta = 0$, OD= 10, $\delta = -1.5\Gamma$, $I_c^+ : I_c^- = $ 25:4, 5:3, 3:5, 4:25. b1)-b4) The result of numerical simulations modeling the effects of intensity imbalance when $\theta = 0$, OD= 10, $\delta = -\Gamma$, $I^+ : I^- = $ 3:2, 5:4, 4:5, 2:3 (note that OD here is defined for unsaturated absorption).

direction parallel to the trapping beams, where A corresponds to the field gradient along the r direction.

The effects of absorption are explicitly included via the z'-dependence of the cooling beam Rabi frequencies. The term $n[z']$ in Eq. 4 corresponds to the integrated position-dependent atomic density at position z', and is determined by counting the number of atoms between the beginning of the trapping volume and position z' along the z'-axis. Because the number of atoms along the z'-direction does not become substantial until the atoms have already been trapped in the radial direction, we only consider the number of atoms very close to the z' axis in our density calculation. It is through the inclusion of this position-dependent attenuation factor that our model differs from previous models and provides a mechanism for intensity-dependent spatial trapping.

A normalized probability ($\bar{P}_i^j$) is calculated for the likelihood of absorption from each beam as

$$\bar{P}_i^j = P_i^j / (P_t^+ + P_t^- + P_c^+ + P_c^-), \tag{5}$$

where $i = (t,c)$, $j = (+,-)$, and P_i^j represents the probability for the absorption of a photon from any one of the laser beams. With these normalized probabilities, a random number in the range [0,1] is used to select which beam is absorbed by each atom. Thus, at each timestep, the positions and velocities of the atoms are appropriately updated, and the integrated density at each point is calculated. We then use this density in the next step to determine the cooling beam attenuation (absorption is ignored along the radial direction because the cloud is always optically thin along this axis). If atoms pass out the trapping region, we consider these atoms to no longer participate in trapping; when this occurs, a corresponding number of atoms with random positions and velocities are placed inside the trapping region. Radiation pressure forces due to rescattering have been ignored due to their lack of importance in an effectively 1D trap [15]. Also, we ignore collisional forces in this model as they present a limitation to trap time and density but are an isotropic effect and therefore do not play a role in determining the trap length or location.
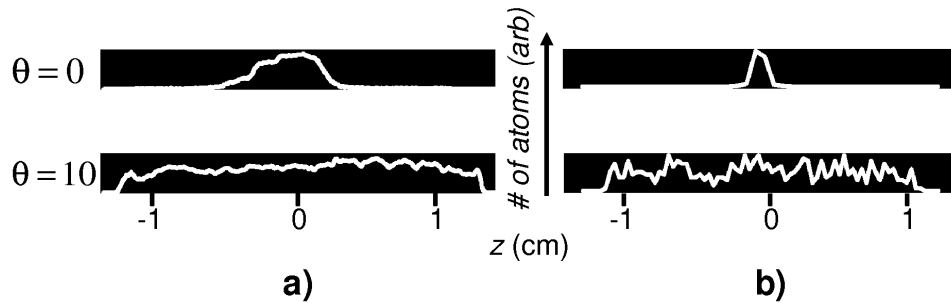
Fig. 4. a) Experimental longitudinal atomic density profiles of traps obtained for equal intensity cooling beams at $\theta = 0°$ and $10°$. b) Numerically modeled atomic density profiles for equal intensity cooling beams at $\theta = 0°$ and $10°$.

4. Results and discussion

In this section, we discuss the effects of absorption-induced trapping and demonstrate both experimental and numerical validations of this mechanism. Furthermore, we detail a method for circumventing the deleterious effects of absorption-induced trapping and present data on our trap.

In order to investigate the effects of absorption-induced trapping, we use an 'ideal' beam geometry where the cooling beams are aligned with $\theta = 0$. We find that we are limited to producing a dense, short trap at a well-specified location. The spatial location of the trap formation is reproducible and depends strongly on the frequency of the trapping lasers and the intensity imbalance of the cooling beams. Furthermore, we can produce a localized trap anywhere along the region of the magnetic-field minimum and transfer atomic populations from one position to the next by varying the cooling-beam intensity imbalance. Figure 3 illustrates the effects of an imposed cooling-beam intensity imbalance on the resulting trap locations. In Figure 3(a), we show experimentally-obatined longitudinal atomic density distributions, where the cooling beams propagate in the horizontal direction. We control the relative intensities of the cooling beams by rotating polarizers placed in the paths of the linearly-polarized cooling beams. From top to bottom, Fig. 3(a) shows the traps that result for decreasing values of $I_c^+ : I_c^-$. Thus, while a trap can be formed anywhere along the region of magnetic-field zero, the trap location is determined by the cooling beam intensity imbalance.

This behavior cannot be accounted for by a model that ignores the absorption of the cooling beams, as a beam imbalance simply acts to provide a net acceleration for the atoms, but would not result in a shifted, stable equilibrium position. As we have already concluded that no magneto-optical trapping occurs along the z-direction, we must consider the effects of absorption on beams propagating along the long axis of the trap in order to explain our experimental results. When the effects of attenuation are considered, our model confirms that spatial trapping should occur and that, as was seen experimentally, the location of the trap depends on the intensity imbalance of the beams. Figure 3(b) illustrates the results of our numerical simulation, with the final positions of an initially randomly distributed group of atoms shown in white. By including both absorption due to the trap and an initial imbalance in the beam intensities, Fig. 3(b) shows that trapping can occur along the region of magnetic-field minimum over a range of several cm, in agreement with our experimental results.

To avoid the effects of absorption-induced trapping, we alter the laser beam geometry to exploit the fact that the trap is optically thick along the longitudinal direction, but is effectively transparent along the transverse direction. This is done by intentionally misaligning the direc-
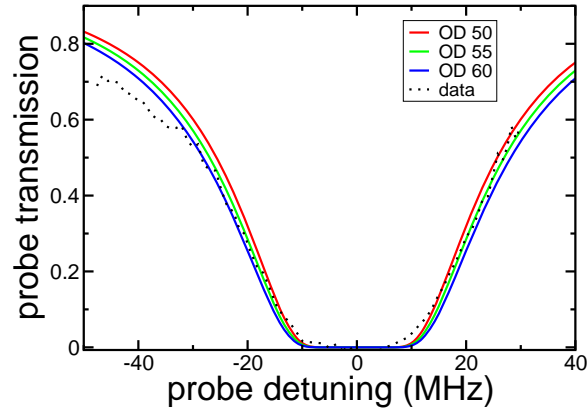
Fig. 5. Measured trap absorption. The absorption is fit using linear absorption theory for a two level atom. The best fit (obtained via a χ^2 fit) corresponds to OD=55 $\pm$ 5.

tion of propogation of the cooling beams with respect to the magnetic-field minimum by an angle θ. The cooling beams still produce effectively an optical molasses to cool the atoms (due to their balanced wave vector components along the z-direction), but now they only traverse an oblique cross section of the trap. Because the trap is optically thin in the transverse direction, the cooling beams' intensities remain balanced throughout the entirety of the trapping region.

Figure 4 shows longitudinal atomic density profiles that result when the cooling beams are of equal intensity and oriented at an angle of $\theta = 0°$ and $10°$. As in Fig. 3, a short trap located in the middle of the trapping region is formed at $\theta = 0°$ but, for $\theta = 10°$, the trap uniformly fills the entire trapping region. Furthermore, we find experimentally that this beam alignment results in a much more robust trap that is more reproducible and less affected by beam misalignments and intensity imbalances. The model results in Fig. 4(b) demonstrate that, despite the presence of absorption-induced, intensity-dependent trapping forces, rotating the cooling beams results in a trap that is spatially unconfined along the magnetic-field minimum. While this technique of intentional 'misalignment' is known to experimentalists [23], this is, to our knowledge, the first detailed study of how this approach improves the resulting trap.

After rotating the cooling beams, we produce a trap with a total length of 3 cm (limited by the length of the cell) and a radius of 0.3 mm (corresponding to an aspect ratio of 100:1). To measure the OD of the trap, we record the transmission spectrum of a weak probe beam ($I_{probe} = 100\,\mu$W, 250 μm beam radius) propagating along the long dimension of the trap with the trap beams turned off. By fitting this spectrum using linear absorption theory (assuming a perfect repump beam), we found that the OD=55$\pm$5. The results of this fit are shown in Fig. 5 and correspond to a density of 7×10^{10} atoms/cm^3 with an effective trap length (defined here as the uniform peak-density region of the trap) of 2 cm. This corresponds to a total of 4×10^8 trapped atoms, which agrees (to within a factor of 2) with the result obtained from the calibrated fluorescence results recorded by the CCD camera. We obtain these results in steady-state working conditions (*i.e.*, we do not use transitory laser beam detunings or magnetic field compression, which have been shown to further enhance the density [16]). Thus, we expect to be able to use these methods to achieve even larger ODs than those reported here.

We use three methods to determine the transverse and longitudinal temperatures of the trap (corresponding to the kinetic energy in the radial and z-direction, respectively). First, the steady state radial size of the MOT was used to determine the transverse temperature of the trap via $T \approx \langle r^2 \rangle \kappa / k_B$ (where κ is the MOT spring constant [24]), which gives a value of 35 μK.

Next, by measuring the decay time of the absorption signal when the trap beams are blocked, a transverse temperature of 28 μK is calculated, which agrees approximately with the previous method. Finally, using the counterpropogating trapping beams as pump beams interacting with a weak probe, we investigated the recoil-induced resonance (RIR) feature seen in our absorption spectra. By fitting the shape of this resonance with the model proposed by Guo *et al.* [25], we obtain effective longitudinal and radial distribution widths (τ_l and τ_r, respectively, as defined in [26]) that are identical to within our measurement accuracy (± 5 μK) and equal to $\sim$30 μK. The fact that these values are close (albeit averaged over the trap length) implies thermodynamic equilibrium and allows us to discuss transverse and longitudinal temperatures. It is worth noting that the atoms are cooled substantially below the Doppler temperature in all directions.

Acknowledgments